

X-ray emission cross sections and spectral distributions for carbon bombarded with MeV C, N, and O ions*

R. K. Cacak[†] and F. W. Martin

Department of Physics and Astronomy, University of Maryland, College Park, Maryland 20742

(Received 2 June 1975)

X rays emitted by a thin target bombarded with C, N, and O ions with energies between 1 and 2.5 MeV are observed at an angle of 135° with a Bragg crystal spectrometer having a resolution of 3 eV. The KL and KL^2 satellite lines of the carbon target are observed, as well as the diagram K line. These peaks are superimposed on a broad x-ray distribution extending from 265 to 290 eV. The KL^2 line appears for N at low energies, but not for C. Projectile and target spectra involve the K and KL lines in approximately equal amounts for C. These observations are interpreted as evidence for a molecular-orbital theory involving promotion of L electrons of the colliding atoms, in which the momentum change of the promoted electron is taken into account. Cross sections for production of carbon K x rays at energies below the carbon absorption edge in the Bragg pseudocrystal are obtained from the data. The cross sections rise monotonically with energy in the range studied and are smallest for oxygen ions, which have the largest atomic number.

I. INTRODUCTION

Atomic collisions which involve atoms lighter than neon as targets and ions heavier than helium as projectiles have several interesting features. First, many theories of excitation and ionization of such target atoms predict a maximum where the velocity of the projectile is equal to the velocity of the bound electron. For low- Z_2 targets it is possible to obtain projectiles equaling or exceeding this velocity with accelerators capable of only a few MeV. It is thus possible to study interaction processes in a region where they should be at a maximum. Second, the mechanisms of interaction at velocities near this maximum are not well understood. Third, the shells in such target atoms are larger than the inner shells in heavier atoms, leading in general to large x-ray cross sections.

Applicable theories fall into two broad schools. One school treats the energy levels of a transient molecule during the collision,^{1,2} but typically does not consider more than two such levels³ nor the momentum change of the promoted electron.⁴ Another school concentrates on the Coulomb force between the nucleus of the projectile and the electrons of the target,⁵⁻⁹ but typically must be modified when $Z_1 \approx Z_2$ in order to account for quasimolecular effects¹⁰ and for screening of the projectile nuclear charge Z_1 by electrons of the projectile.¹¹

Experiments with light targets offer an opportunity for testing improvements of these theories in cases where relatively few electrons are involved. Relatively few experiments involving the x rays emitted during such collisions have been made, primarily because the x-ray energies are

below those detected efficiently by Si(Li) semiconductor detectors. Proportional-counter measurements have been made of the x rays emitted after collisions of high-velocity heavy ions with energies less than 80 keV,¹² 150 keV,¹³ and 1.5 MeV,¹⁴ and spectral measurements have been made on Ar and CH₄ targets for ions with $Z_1 > 10$ in the keV region.^{15,16} Spectral measurements generally provide much more information about the nature of the collision processes; for example, they enable determination of the states of ionization of the L shells of the collision partners.

The measurements to be described below have been made with a Bragg crystal spectrometer, which enables complete separation of x rays emitted by the target from those emitted by the projectile, e.g., N and O K x rays. In addition, the spectrometer is capable of resolving the Doppler-shifted x rays from the C projectile and the satellite x rays emitted by carbon ions in the target or the beam with various numbers of L -shell vacancies. The present experiments extend cross-section and spectral measurements for C, N, and O ions bombarding a C target up to 2.5 MeV, and provide evidence that certain aspects of these collisions must be described in terms of transient molecular effects even though the projectile has a very high velocity for these effects.

II. EXPERIMENTAL PROCEDURE

A. Apparatus

Equipment consisted of a 3-MV Van de Graaff accelerator, magnetic and electrostatic analyzers, collimating system, thin carbon target, Bragg pseudocrystal soft-x-ray spectrometer, semi-

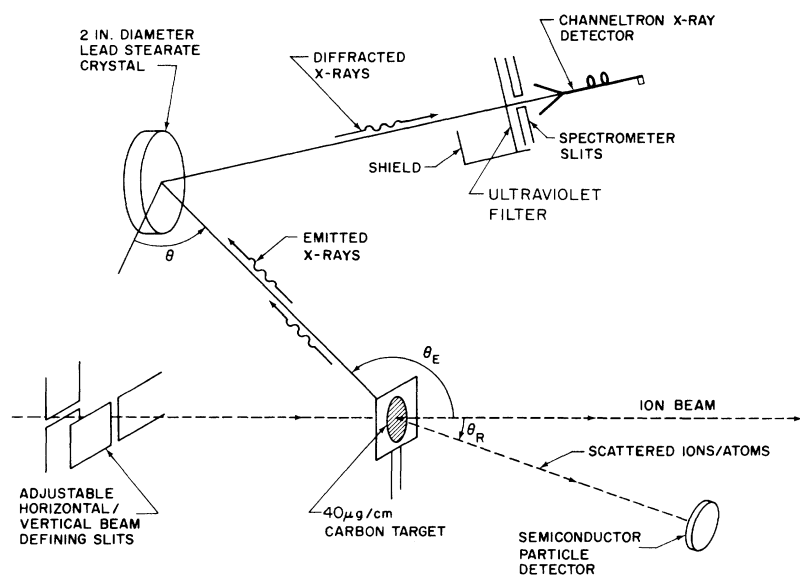


FIG. 1. Schematic diagram of the experimental setup. Ion-beam current is not used as an experimental parameter. X-ray counts at a given Bragg angle are accumulated in a multichannel analyzer until a preset number of scattered ions are counted, at which time the Bragg angle and the analyzer address are incremented. The cycle is then repeated, producing an x-ray spectrum in the analyzer.

conductor particle detector, and auxiliary beam-current monitor. The acceleration and identification of C, N, and O ions has been described elsewhere.¹⁷ Ions emerging from the electrostatic analyzer could reach the target through two square collimators, 1.6 and 1.3 mm on a side. The two collimators were 3.4 m apart and the smaller collimator was 1.7 m from the target. These collimators, designed for differential-scattering measurements, served to prevent ions from striking the thick frame of the target holder or other sensitive parts of the apparatus. The second collimator consisted of slits independently adjustable while under vacuum in vertical and horizontal directions. These slits were adjusted by maximizing the counting rate in the x-ray spectrometer.

The collision chamber housed all components except the collimators, as shown schematically in Fig. 1. The chamber was a cylinder, about 61 cm in diameter and 24 cm in height, constructed mostly of aluminum. Clean vacuum techniques were employed to reduce the possibility of contamination of the pseudocrystal or the secondary-electron-emitting surfaces in the x-ray detector. Ungreased, baked, Viton O-rings were used on most static seals; grease with a vapor pressure of 10^{-10} Torr was used elsewhere. A cold trap cooled with liquid nitrogen was used to baffle the 6-in. diffusion pump, and a polyvinyl-ether-type oil was used in both the diffusion pump and the forepump.

The target was a film of carbon with a thickness of about $40 \mu\text{g}/\text{cm}^2$, suspended on a holder attached to the central shaft of the x-ray spectrometer. By rotating the central shaft, the angle between the

beam and the foil normal could be adjusted. The energy loss of ions passing through the foil was about 100 keV.

Near the floor of the chamber, a rotating table was provided to which a structure supporting a semiconductor particle detector could be attached. The table could be rotated under vacuum, so that the angle θ_R through which the ions and atoms were deflected could be changed. The detector was located at $\theta_R = 32^\circ$ and was collimated to subtend 1.26×10^{-4} sr. This detector was used to measure the product of the target thickness and incident ion current, as described below.

The spectrometer was a double-focusing device specially designed to analyze collision-induced x rays, utilizing a lead stearate pseudocrystal deposited on a spherical concave glass lens.¹⁸ The x rays emitted at an angle θ_E relative to the direction of the ion beam were Bragg reflected from the pseudocrystal into a channeltron electron multiplier, which is sensitive to both vacuum ultraviolet (vuv) radiation and soft x rays. A thin film of silver was used as a filter to eliminate vuv radiation and to transmit soft x rays with about 30% efficiency throughout the wavelength region of interest.¹⁹ In this spectrometer the Bragg angle θ may be varied while θ_E is fixed. For the results to be presented, $\theta_E = 135^\circ$.

Most of the ions passed through the target and were collected in a Faraday cup located 2.5 m from the target. The sum of the currents at the Faraday cup and target was monitored only as an aid in optimizing accelerator operation. No suppression of secondary electrons was attempted. Typical measured currents were 10–50 nA.

B. Scattered and recoil particle counting

For thin targets, the x-ray cross section is given by

$$\sigma_x = 4\pi \frac{(d\sigma/d\Omega)\Omega_R X_T \Delta\theta}{\epsilon_x \Omega_x R \tau}, \quad (1)$$

in which $d\sigma/d\Omega$ is the differential cross section for Rutherford scattering of particles at the angle θ_R , Ω_R is the solid angle subtended by the semiconductor detector, X_T is the integrated number of channeltron counts in a spectrometer peak, $\epsilon_x \Omega_x$ is the product of the spectrometer efficiency and solid angle, R is the number of particle counts per step of the spectrometer, $\Delta\theta$ is the angular increment in θ per spectrometer step, and τ is the angular width of the spectrometer slits.²⁰ In the derivation of Eq. (1) the target thickness and particle current divide out, and it therefore provides a means of comparing measurements from one ion energy to another and from one ion to another without measuring the former quantities. The present section presents the factors in Eq. (1) relative to particle counting.

Because projectiles which were Rutherford scattered and target atoms which were knocked from their original position had approximately the same energy, the semiconductor detector did not discriminate between them. The cross section for production of both scattered and recoil particles is

$$\frac{d\sigma}{d\Omega} = \frac{d\sigma}{d\Omega_s}(\theta'_s) \frac{d\Omega'_s}{d\Omega}(\theta'_s) + \frac{d\sigma}{d\Omega_r}(\pi - \theta'_r) \frac{d\Omega'_r}{d\Omega}(\theta'_r), \quad (2)$$

where the Rutherford cross section in the center of mass coordinates is

$$\frac{d\sigma}{d\Omega_s}(\theta'_s) = 1.296 \times 10^{-3} \left(\frac{Z_1 Z_2}{E} \right)^2 \left(\frac{m_1 + m_2}{m_2} \right)^2 \csc^4\left(\frac{1}{2}\theta'_s\right) \quad (3)$$

in units of b/sr,²¹ and the center-of-mass transformation formulas are given by

$$\frac{d\Omega'_s}{d\Omega}(\theta'_s) = \frac{[(m_1/m_2)^2 + 2(m_1/m_2) \cos\theta'_s + 1]^{3/2}}{(m_1/m_2) \cos\theta'_s + 1} \quad (4)$$

for the scattered projectile,²² and

$$\frac{d\Omega'_r}{d\Omega}(\theta'_r) = 2^{3/2}(1 + \cos\theta'_r)^{1/2} \quad (5)$$

for the recoil atom. In these expressions Z_1 and m_1 are the atomic number and mass of the projectile, Z_2 and m_2 are the corresponding quantities for the target atom, E is the laboratory energy of the projectile in MeV, θ'_s is the center-of-mass angle of the scattered projectile, and θ'_r is the center-of-mass angle of the recoil atom.

In Eq. (2) the Rutherford cross section $d\sigma(\theta'_r)/d\Omega'_r$ for producing recoil atoms at the angle θ'_r , such that they travel at an angle θ_R in the laboratory, has been replaced by the Rutherford cross section $d\sigma(\pi - \theta'_r)/d\Omega'_s$ for scattering projectiles at an angle 180° from θ'_r . The angle θ'_s and the laboratory scattering angle are related by

$$\sin(\theta'_s - \theta_R)/\sin\theta_R = m_1/m_2, \quad (6)$$

while the corresponding relation for θ'_r is

$$\theta'_r = 2\theta_R. \quad (7)$$

Equation (2) was evaluated for the value $\theta_R = 32^\circ$ used, giving values of $E^2 d\sigma/d\Omega$ of 8.06, 342, 463 and 782 (MeV)²b/sr for H, C, N, and O ions colliding with carbon, respectively. The percentages of particle counts owing to recoiling heavy ions were between 13% and 17%.

C. Spectrometer transmission

In order to determine the spectrometer transmission $\epsilon_x \Omega_x$ at the Bragg angles used, Eq. (1) was applied to measurements of the x rays produced by 1.0-MeV protons, for which the value of σ_x can be computed. The measured proton-induced x-ray spectrum is shown in Fig. 2. The total number of counts above background in this spectrum was taken as X_T , and $\sigma_x = \omega\sigma_A$ was evaluated from the fluorescence yield²³ $\omega = 0.0022$ and the cross section $\sigma_A = 1.08 \times 10^{-18}$ cm² for emission of Auger electrons²⁴ at 1 MeV. The value of $\epsilon_x \Omega_x$ obtained by inverting Eq. (1) was 2.05×10^{-7} sr,

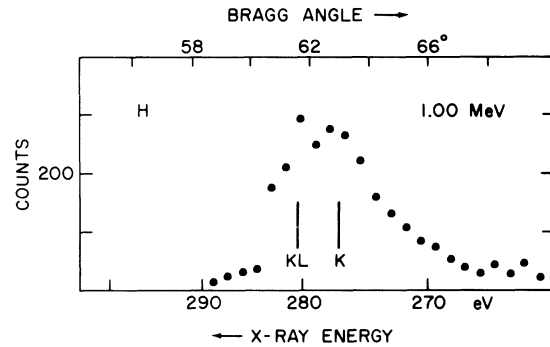


FIG. 2. Soft-x-ray spectrum of an evaporated carbon film excited by protons with 1-MeV incident energy. Absolute number of x-ray counts is plotted vs Bragg angle (upper scale) and against x-ray energy (lower, nonlinear scale). The statistical counting error in the vertical scale varies as the square root of the number of counts and is about ± 14 at 200 counts; the error in Bragg angle is about 0.1° . The same scales are used in Figs. 3-5, and error bars have been omitted throughout for clarity. Long lines in the figure also have the same positions as the long lines in Figs. 3-5. The peak marked *KL* is ascribed in the text to a combination of a *KL* satellite line and *K* emission associated with the π band of graphite.

with a probable error of 25%, estimated as 10% in X_T , 10% in ω , and 20% in σ_A .

Constant settings of the spectrometer slit width W , the step width $\Delta\theta$, and the angle between foil and beam were used for measurements with both protons and heavy ions. The best angle for the foil is theoretically one in which the plane of the foil points at the pseudocrystal; however, at this angle the foil holder intercepts emitted x rays. Too large a rotation from this angle would induce an error, since the size of the beam spot on the foil, as viewed from the pseudocrystal, would exceed the allowed source width w .²⁵ The angle was chosen so that the maximum possible size of the beam spot, as calculated from the collimating-slit dimensions, was equal to w .

III. RESULTS

Spectra produced by various ions bombarding carbon are shown in Figs. 2-5. The intensity

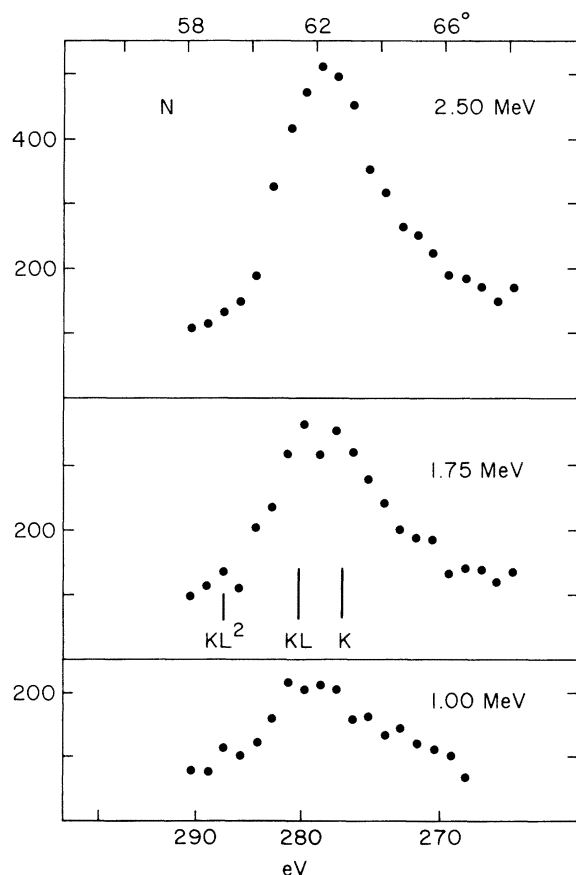


FIG. 3. Soft-x-ray spectra of a carbon film excited by nitrogen ions incident with three different energies. The peak marked KL^2 is at a greater energy than observed for electron-excited spectra and is attributed to carbon atoms with two L -shell vacancies at the time of x-ray emission.

plotted as a function of Bragg angle θ is shown in Fig. 2 for protons, in Fig. 3 for nitrogen ions, in Fig. 4 for carbon ions, and in Fig. 5 for oxygen ions. The data have been smoothed slightly by summing $X(\theta_i)$ for five steps with $\Delta\theta = 0.1^\circ$. Each portion of each figure corresponds to an arbitrary number R of particle counts per step.

Cross sections were computed from the data shown in these figures by evaluating the number X_T of counts above background and above θ_A , where θ_A is the Bragg angle corresponding to the K absorption edge of carbon atoms in the lead stearate crystal. Backgrounds were evaluated from the counting rates far from the peaks in the spectra, and an experimental estimate of θ_A was made by averaging the Bragg angles which have greatest slope in the region $60^\circ < \theta < 61^\circ$. Energies determined from the voltage on the electrostatic analyzer¹⁷ were corrected to the center of the foil using stopping-power data²⁶ and the foil thickness

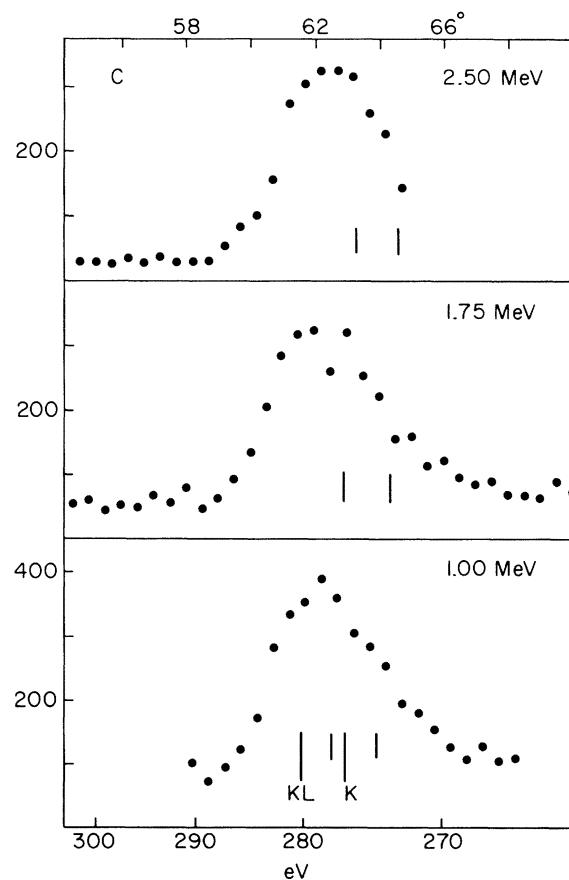


FIG. 4. Soft-x-ray spectra of a carbon film excited by carbon ions incident with three different energies. The short vertical lines mark the positions at which x rays with the energies of the long lines would appear, on account of the Doppler shift, if they were emitted by the carbon projectile.

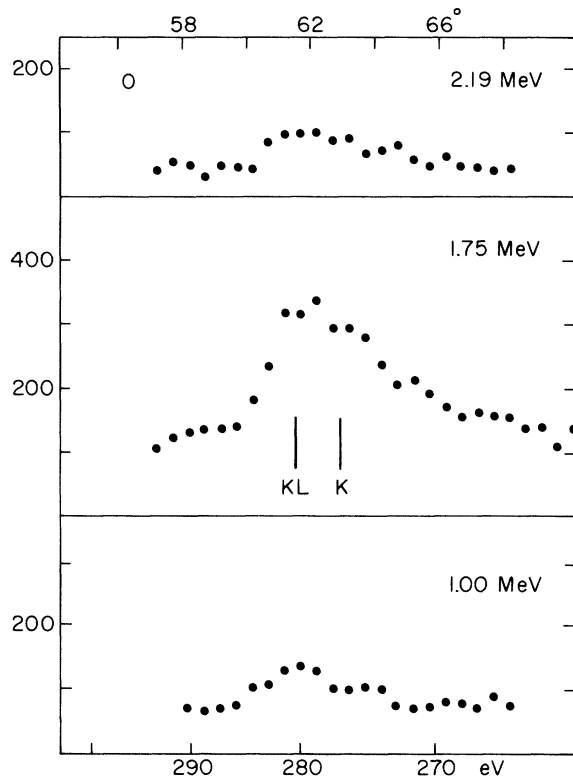


FIG. 5. Soft-x-ray spectra of a carbon film excited by oxygen ions incident with three different energies.

of $40 \mu\text{g}/\text{cm}^2$. Corrected energies were used in evaluating Eqs. (3) and (1). Cross sections computed in this way are listed in Table I and shown in Fig. 6 as functions of ion energy. Because none of the parameters in Eq. (1) were changed except X_T and R , relative errors should reflect only the uncertainties in X_T , estimated as 16%. Absolute cross sections have a probable error of 25%, mostly associated with the uncertainty in $\epsilon_x \Omega_x$.

TABLE I. Cross sections $\sigma_x(E)$ for emission of carbon K x rays (having energies below the absorption edge of lead stearate) by an evaporated carbon foil bombarded with ions of energy E .

Projectile	E (MeV)	$\sigma_x(E)$ (10^{-21} cm^2)
C	0.92	29.0
	1.63	47.1
	2.35	49.7
N	0.88	25.9
	1.60	30.7
	2.33	39.4
O	0.88	9.0
	1.59	13.4
	2.02	19.3

IV. DISCUSSION

A. Spectral lines

The simplest spectrum is that excited by 1.0-MeV protons, shown in Fig. 2. A broad distribution from about 265 to 290 eV is apparent, with two peaks visible near 280 eV. Similar peaks are apparent in Figs. 3 and 4 for N and C ions at 1.75 MeV. The fact that the valley between these peaks nearly disappeared when the angular width τ of the detector slit in the spectrometer was increased from 0.50° to 1.1° is an experimental indication that the angular width of the diffracted x-ray beam was less than 1.1° . The corresponding energy resolution²⁷ is less than 2.7 eV. A typical value for a lead stearate analyzer in which 100 layers participate in diffraction at second order is 2.7 eV.²⁸

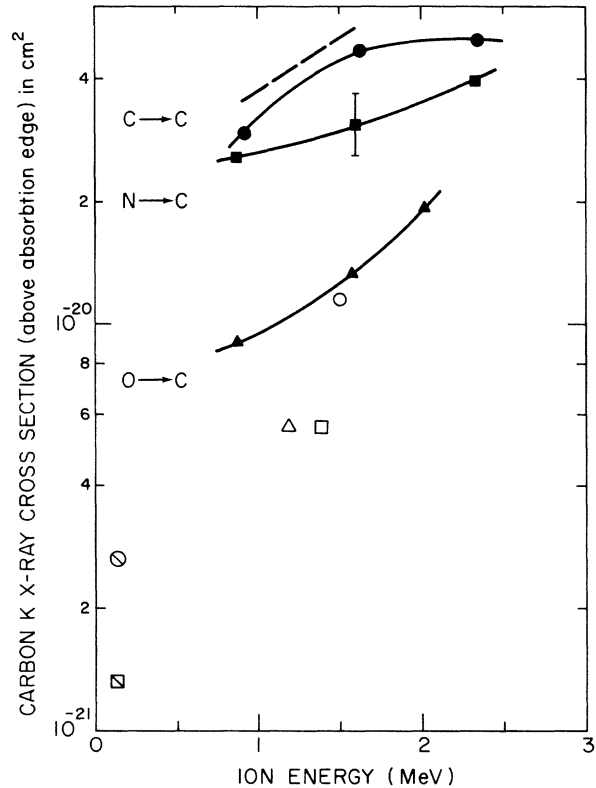


FIG. 6. Cross section for production of carbon K x rays with energies below the absorption edge of lead stearate by ions with laboratory energies (at the mid-plane of the target) between 0.8 and 2.4 MeV. Circles, squares, and triangles are used for C, N, and O ions, respectively. Filled symbols show the present results. For comparison the highest-energy cross sections of Ref. 13 for a methane target and of Ref. 14 for a carbon target are plotted as open symbols with and without diagonal bars, respectively. The dashed line is computed as described in the text from the theory of Briggs and Macek (Refs. 3 and 46) for $\text{C} \rightarrow \text{C}$. The solid lines are drawn by hand through the present results and a typical error bar is shown.

TABLE II. Experimental energies E_{ex} , satellite configurations, theoretical fluorescence yields ω_K , and theoretical and experimental energy shifts ΔE from the diagram line.

E_{ex}^a	Satellite	Vacancy configuration	ω_K	ΔE_{th}^b	ΔE_{ex}^a
276.7	K	[1s]	0.0026 ^c	0	0
280.5	KL	[1s, 2p]	0.0022 ^c	4.7	3.8
		[1s, 2s]	0.0065 ^c		
287.0	KL^2	[1s, 2p ²]	0.00 ^c	10.4	10.3
		[1s, 2s ²]	0.0138 ^c		
		[1s, 2s, 2p]	0.0122 ^c		
	KL^3	[1s, 2s, 2p ²]	1	17.2	
		[1s, 2s ² , 2p]	1		

^a Present experiment.

^b F. P. Larkins (private communication). See also Ref. c below.

^c L. H. Toburen and F. P. Larkins, Phys. Rev. A **6**, 2035 (1972).

These considerations show that the resolution of the spectrometer is good enough to measure the spectral distribution of emitted x rays, which would be expected to extend over the theoretically computed width of about 14 eV for the filled bands of graphite.²⁹

The spectra do in fact have peaks at nearly the same locations as the soft-x-ray spectra of graphite excited by electrons. Table II lists the energies corresponding to the longer vertical lines marked in Figs. 2–5 as calculated from the Bragg equation using a $2d$ value of 100.6 Å. The peak at 276.7 eV does correspond closely with the previously determined maxima at 276 eV (Ref. 30) or 276.6 eV (Ref. 31). Previous spectra have been analyzed into a number of subpeaks, four of which are interpreted³² as corresponding to the three σ bands and the single π band of graphite. The subpeak at 276 eV and the two adjacent subpeaks are assigned to the σ band having wave functions within the parallel planes of the graphite structure formed from the 2s, 2p_x, and 2p_y electrons of carbon. An additional subpeak at 281 eV (Ref. 30) or 280.6 eV (Ref. 31) is assigned to the π band, which has wave functions formed from the 2p_z atomic orbital that bridges the space between the planes of graphite. The energy of this peak corresponds quite well with the value of 280.5 eV listed for the second peak of the present spectra in Table II. Thus the two peaks might be caused by the σ and π bands of graphite.

However, the intensity near 281 eV in previous measurements is about 20% (Ref. 30) or 50% (Ref. 31) of the intensity near 276 eV, while in the present measurements the 281- and 276-eV peaks are

nearly equal in intensity. It is reasonable to infer that the 1-MeV protons, which have a lower velocity than 4-keV electrons, are interacting with graphite atoms in a somewhat different manner than electrons. In addition it is known from studies of Auger electrons emitted by gaseous targets that 600-keV protons produce carbon ions with simultaneous K - and L -shell vacancies more effectively than carbon ions with only K -shell vacancies,³³ and that the probability of double ionization increases as the proton energy is reduced below 0.6 MeV in similar cases.³⁴ The energy of K x rays emitted by such doubly ionized atoms is slightly increased because the reduced screening increases the binding of K electrons more than that of L electrons, producing KL satellite lines. The calculated shift ΔE_{th} in energy of such satellite lines from the “diagram” line emitted by the atom with one K vacancy is listed in Table II, and is in reasonable agreement with the experimental shift ΔE_{ex} from the experimental peak of lowest energy. It therefore seems reasonable to attribute the additional intensity observed in the present spectra near 281 eV to KL satellite emission involving L electrons from the σ band. Satellite emission involving L electrons from the π band should, on this model, occur near 284 eV and have an intensity of (20–50)% of the satellite contribution to the peak near 281 eV, and should therefore not be statistically significant in the spectra.

The spectrum for nitrogen ions, shown in Fig. 3, is more complicated. The K and KL lines are clearly visible. In this case a clear indication of a third peak is also seen at about 287 eV. If the spectrometer efficiency is considered, the intensity of this line may be estimated as perhaps 30% of the total intensity at 1.75 MeV. Its energy corresponds approximately to the calculated energy listed in Table II for the KL^2 satellite, emitted by atoms with two initial L -shell vacancies. It is difficult to advance a solid-state explanation for this line, since the maximum energy of a transition from the valence band is 285.6 eV.³¹ Although simultaneous production of a K vacancy and excitation of electrons to the conduction band has been proposed in connection with satellite spectra,³⁵ it is difficult to see how this mechanism could produce a line of the observed energy, since graphite has no energy gap.²⁹ The peak at 287 eV therefore is interpreted as a KL^2 satellite line emitted by solid carbon.

Spectra produced by carbon ions are the most complicated and are shown in Fig. 4. The two lines in the proton-induced spectrum are present, as well as emissions from the moving carbon ion that are Doppler shifted. The wavelength associated with radiations from the moving ion is dif-

difficult to determine, being the result of two effects: (i) Screening of the K electrons by any electrons bound to the projectile, which will be different than the screening of stationary atoms by electrons in the valence band of the solid, and (ii) some sort of dynamic screening of the K electrons by electrons in the valence band, set up as the projectile moves through the electron gas of the solid. If it is assumed that the result of these effects is no shift of the radiation from a given configuration of the projectile (measured in its rest frame) from that of the same configuration of the target, the wavelengths of the Doppler-shifted radiations from the projectile may be determined. The calculated positions of the shifted lines are drawn as short vertical lines in the figure. Since the spectra were obtained with $\theta_E = 135^\circ$, the wavelengths and Bragg angles of radiations emitted by moving ions are shifted towards larger values as the energy of the ions is increased. Note that at 1.75 MeV the shifted KL line apparently lies near the position of the unshifted K line, and both emissions contribute to the intensity of the right-hand peak. Also, at 2.50 MeV the energy of the KL^2 line seems to have shifted enough so that it is beginning to be reflected efficiently by the lead stearate pseudocrystal, and the shifted KL^2 line appears as a shoulder on the left-hand side of the main distribution at about 60° .

Data for oxygen ions are not available with enough statistical significance to draw conclusions as to line position. Spectra are shown in Fig. 5. In all the figures the long lines marked K and KL have the positions given in Table II.

B. Intensities of satellite lines

It is remarkable that the KL^2 satellite line appears strongly only when N ions are used as projectiles. Furthermore, the relative excitation of this satellite is greatest at low energies. These observations may be qualitatively explained by invoking a two-state molecular-orbital theory of the collision,³⁶ in which the coordinate axes are fixed in the laboratory and in which the high velocity of the projectile is treated using molecular orbitals which contain a momentum factor in the separated-atom limit.³⁷ This theory contains the usual variation of adiabatic molecular energy levels as a function of distance, in which the levels can have permitted or avoided crossings depending on their symmetry classes. If carried through without neglecting the rotation of the internuclear axis, this theory gives the usual coupled equations for the state amplitudes as the system passes through a crossing, with the addition of a factor $\exp(imVz/\hbar)$ in the matrix element, where z is the coordinate of the active electron in the direction of \vec{V} . Al-

though this factor may remove the distinction between rotational and radial coupling, interpretation can be carried out simply under the assumption that crossings exist and that transitions with a reasonable velocity dependence occur at the crossings when one of the levels involved is vacant.

The correlation diagram¹ for N→C collisions, as shown in Fig. 7, contains three curve crossings that may be relevant for promotion of L -shell electrons of C: (a) $3d\pi - 3d\sigma$ at $R \rightarrow 0$; (b) $3p\sigma - 3p\pi$ at $R \rightarrow 0$; and (c) $4f\sigma -$ (many levels at various radii). The transition $3p\sigma - 2p\pi$ by rotational coupling, which would act in the same way as transition (a), is not expected to be strong at large internuclear separations.³⁸ Inside the foil the N atom has an average of four electrons bound to it, possibly in a $1s^2, 2s^2$ configuration.³⁹ The $3d\sigma$ molecular level formed from the $2p(N)$ level then has a high probability of being vacant, so that "demotion" of an electron from the $2p(C)$ level is allowed. The other processes [(b) and (c)] connect the $2p(C)$ and $2s(C)$ levels with unoccupied levels having principal quantum number 3, so that promotion from these levels is allowed. Thus all these processes can lead to ionization of the carbon L shell.

In the case of C→C collisions the correlation diagram¹ no longer has separate levels for the L shells of the projectile and target at large R . How-

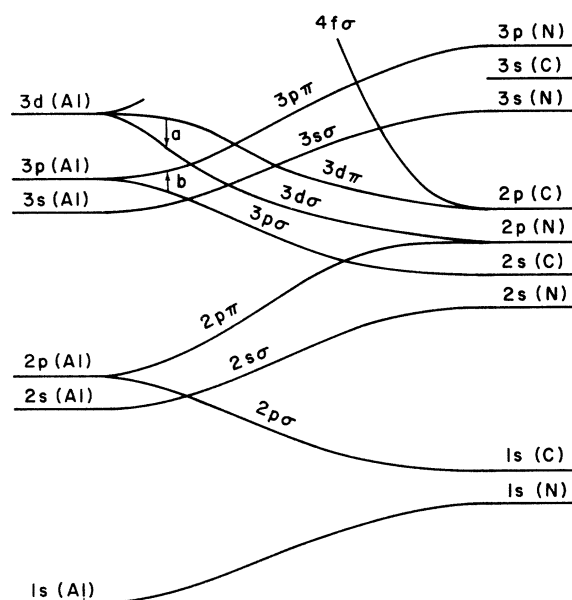


FIG. 7. Correlation diagram for N→C collisions, taken from Fig. 5 of Ref. 1. The stripped nitrogen ion within solid carbon has several vacancies in the $2s(N)$ or $2p(N)$ levels. It is proposed in the text that transition (a) accounts for the KL^2 satellite line of carbon observed in connection with N→C collisions.

ever, the $2s(C)$ and $2p(C)$ levels split into separated levels with the same quantum numbers (except for parity) as the asymmetric case, so that transitions may still occur at curve crossings (a), (b), and (c). Transitions of type (a) simply return the demoted electron to one shell of the collision partners. Thus the principal difference between C-C and N-C collisions is that crossings of type (a) remove carbon L -shell electrons only in the N-C collision.

Before applying this model to the data, a reasonable velocity dependence for the transitions at the three curve crossings must be determined. In general the factor $\exp(imVz/\hbar)$ which appears in high-velocity atomic and molecular collision problems has a simple interpretation.⁴⁰ This factor causes the transition probability to decrease as the initial momentum distribution of the active electron in its initial wave function has progressively smaller overlap with the distribution of its final wave function, which is centered at a distance $m\bar{V}$ away from the center of its initial distribution in momentum space. Thus it expresses conservation of momentum of the active electron. The velocity at which the transition probability begins to fall may be estimated by considering the spatial region $-a < z < a$ in which the overlap of initial and final wave functions is large. Matrix elements involving the exponential factor are then made small by its oscillatory behavior unless $mVa < \hbar = mv_0a_0$. The maximum overlap of wave functions will occur when $\vec{R} \cdot \vec{V} = 0$ and will extend to the dimension of the wave functions of states involved in the curve crossing. When the crossing involves the wave functions of the united atom, this dimension may be estimated as $a = n^2a_0/Z_s$, where n is the principal quantum number and Z_s is the screened nuclear charge⁴¹ in the united atom. The velocity at which the transition probability begins to fall is then given by

$$V_m = Z_s v_0 / n^2. \quad (8)$$

For curve crossings (a)-(c) which involve the M shell of Mg or Al, V_m is about $0.3v_0$. The velocity of 1- and 3-MeV carbon ions is 5.4 and 9.5 times this velocity, respectively. Thus it may be reasonably expected that whatever transitions occur at curve crossings in the M shell of the united atom at 1 MeV will be appreciably less probable at 3 MeV.

Consider now the electron population of the L shell of C in N-C collisions. Inside the solid, the charge state of the moving N ion will be +2 or +3 at low velocities,³⁹ and there will be five or six vacant levels in the nitrogen L shell, so that transition (a) is not forbidden. At low velocities, transitions may be assumed to occur at all three curve

crossings, with the result that two electrons can be removed from the carbon L shell, thereby producing the KL^2 line. At high velocities the transition probability decreases, accounting for the disappearance of the KL^2 line.

Consider in addition the somewhat different case when carbon ions are projectiles. The charge state of the ion within the solid is again +2 or +3 at low velocities, leading to six or seven electrons in the L shells of the separated atoms (after promotion of one K electron), or to five or six electrons if one electron is removed because of transitions (b) and (c). Assuming these electrons are shared among the collision partners, as the molecular-orbital model predicts, most of the resulting separated atoms will have three L -shell electrons, leading to predominantly KL satellites in both target and projectile, as observed. If the projectile did not capture electrons, as is assumed to be the case by typical Coulomb ionization theories, it would be expected to retain its +2 or +3 charge state, and to emit the KL^2 and KL^3 satellite lines, which are not observed at low velocities. Finally, as the velocity is increased, transitions of types (b) and (c) will become less probable in the same way as for N-C collisions, so that the possibility of five electrons in the L shells after a collision initiated by a C^{+3} ion is less likely, and the KL^2 satellite should not be observed. However, at 2.5 MeV there is a 34% probability of C^{+4} ions for the ion beam inside the solid,³⁹ and in molecular theory the +4 ions again lead to five electrons in the L shells and production of KL^2 satellites. These KL^2 radiations from the projectile can then be Doppler shifted below the absorption edge, as seems to be observed. If the C^{+4} projectiles captured only a single electron, KL^3 satellites would be expected from the projectile, again a radiation which is not observed at 2.5 MeV.

The two-state approximation is not a sufficient one for exact description of these collisions. For collisions with $n = 2$ in the united atom, it is known both theoretically and experimentally that transitions to molecular states of proper symmetry with energies in the continuum occur in appreciable amounts as the projectile velocity increases.⁴² Thus the above discussion cannot take account of possible vacancy production by direct ionization. However, it does give evidence that a description in terms of crossing of molecular levels, rather than a Coulomb ionization theory, accounts for part of the vacancy production. Without a molecular model, it is very difficult to explain the production of the KL^2 satellite by N and not by C ions, and to explain the lack of a marked difference between projectile and target spectra in C-C collisions.

C. Cross sections

The data shown in Fig. 6 may be compared with other experimental data and with the predictions of molecular and Coulomb ionization theories. The figure shows the highest cross section found in a previous low-energy measurement.¹³ Also shown are previous data¹⁴ up to 1.5 MeV, which are about a factor of 4 lower than the present measurements. Corrections to data on these collision systems on account of recoil effects are not large.⁴³ However, the previous data were normalized to measurements of the proton-induced cross section by Khan, Potter, and Worley,⁴⁴ which have been found to be about a factor of 4 lower than later measurements by two groups using 100-keV protons and solid carbon.⁴⁵ Half of this factor is due to error²³ and the remainder remains unexplained. Regardless of exact cause, however, the normalization factor based on Ref. 44 which was used in Ref. 14 appears to be incorrect by approximately the amount required to explain the difference between previous and present measurements.

Figure 6 contains a dashed line calculated for C-C collisions from the scaled vacancy-production cross sections of Briggs and Macek,³ using a total number of ten vacancies in the *L* shells of the collision partners⁴⁶ and a fluorescence yield of 0.003 (estimated from the spectra of Fig. 4 and the calculated fluorescence yields of Table I). This theory approximates the experimental values at the extreme upper end of its range, a behavior which has been found recently for Al and Ni symmetric collisions.⁴⁷

The data have also been compared to a Coulomb ionization theory in which the increased binding of the target *K*-shell electron during the collision is taken into account.⁹ Although this theory is invalid for $Z_1 = Z_2$, it can perhaps be taken as a lower limit, as polarization corrections increase the vacancy-production cross section in the "positive- Z_1^3 region" below the maximum in the uncorrected theory.^{9,10} With a value of $\omega_K = 3.4 \times 10^{-3}$ estimated from the spectra, a cross section $\omega_K \sigma_K^B$ of 2.2×10^{-21} cm² is obtained from the theory for 2.5-MeV C ions. This is in fact below the experimental result. As σ_K^B has its maximum at about 21 MeV for C-C, and the polarization correction appears to increase the cross section by as much

as a factor of 10 at energies an order of magnitude below that of the uncorrected maximum,¹⁰ it appears that modification of the Coulomb theory to account for polarization effects may cause it to agree with the present data.

An effect which is suggestive of a molecular model is the decrease of the cross sections with the atomic number of the projectile. For example, 1.6-MeV O ions have a smaller cross section than 1.4-MeV N ions, and the latter have a smaller cross section than 1.2-MeV C ions, while all these ions have 0.1 MeV/amu of energy per unit mass. This dependence would not be predicted by a simple Coulomb theory, in which the cross section is proportional to Z_1^2 at constant velocity. While the binding correction⁹ does cause σ_K^B for oxygen to decrease to 49% of σ_K^B for carbon, the polarization cross section causes an increase, and the net effect may perhaps be more simply computed using a molecular theory.

V. SUMMARY

Ion-induced *K*-x-ray satellite spectra have been observed from thin-film carbon targets. The energies of peaks ascribed in whole or in part to satellites are in reasonable agreement with theoretical calculations.⁴⁸ The differing spectra excited by C and N ions and the lack of marked difference between projectile and target spectra for C-C collisions are interpreted as evidence for formation of transient molecular states from the *L* shells of the collision partners, even though electrons in these shells have velocities as much as 30% lower than the projectile velocity. The cross sections for *K*-x-ray production (for x rays with energies above the absorption edge of carbon) are most nearly in accord with the theory of Briggs and Macek, which involves promotion of an electron from the $2p\sigma$ to $2p\pi$ state of the transient molecule formed from the *K* shells of the collision partners by rotational coupling at small impact parameters.

VI. ACKNOWLEDGMENTS

We thank Dr. Song Sik Choe for his help in the early stages of this work, and W. Schaefer for his assistance at the Van de Graaff accelerator.

*Work partially supported by the Energy Research and Development Administration under Contract No.

AT(11-1) 2454 and by the Office of Naval Research under Contract No. N00014-67-A-0239-0026.

†Present address: University of Colorado Medical

Center C-278, 4200 E. Ninth Ave., Denver, Colo. 80220.

¹M. Barat and W. Lichten, *Phys. Rev. A* **5**, 211 (1972).

²Q. C. Kessel and B. Fastrup, *Case Stud. At. Collis.* **3**, 137 (1973).

- ³J. S. Briggs and J. H. Macek, *J. Phys. B* **6**, 982 (1973).
- ⁴D. R. Bates, *Proc. R. Soc. A* **257**, 22 (1960).
- ⁵E. Merzbacher and H. W. Lewis, *Encycl. Phys.* **34**, 167 (1958).
- ⁶G. S. Khandelwal, B. H. Choi, and E. Merzbacher, *At. Data* **1**, 103 (1969).
- ⁷J. D. Garcia, *Phys. Rev. A* **4**, 955 (1971), and references therein.
- ⁸J. H. McGuire and P. Richard, *Phys. Rev. A* **8**, 1374 (1973).
- ⁹G. Basbas, W. Brandt, and R. Laubert, *Phys. Rev. A* **7**, 983 (1973).
- ¹⁰W. Brandt, in *Proceedings of the International Conference on Inner Shell Ionization Phenomena and Future Applications, Atlanta, Georgia, 1972*, edited by R. W. Fink, S. T. Manson, J. M. Palms, and P. V. Rao, CONF-720404 (Natl. Tech. Information Service, U. S. Dept. of Commerce, Springfield, Va., 1972), Vol. 2, p. 975; see Fig. 14.
- ¹¹D. Burch, N. Stolterfoht, D. Schneider, H. Wieman, and J. S. Risley, *Phys. Rev. Lett.* **32**, 1151 (1974).
- ¹²F. W. Saris, *Physica (Utr.)* **52**, 290 (1971).
- ¹³H. Tawara and F. J. De Heer, *Physica (Utr.)* **68**, 607 (1973).
- ¹⁴R. C. Der, R. J. Fortner, T. M. Kavanagh, and J. M. Khan, *Phys. Rev. A* **4**, 556 (1971); R. J. Fortner, B. P. Curry, R. C. Der, T. M. Kavanagh, and J. M. Kahn, *Phys. Rev.* **185**, 164 (1969).
- ¹⁵M. E. Cunningham, R. C. Der, R. J. Fortner, T. M. Kavanagh, J. M. Khan, C. B. Layne, E. J. Zaharis, and J. D. Garcia, *Phys. Rev. Lett.* **24**, 931 (1970).
- ¹⁶R. J. Fortner, *Phys. Rev. A* **10**, 2218 (1974).
- ¹⁷F. W. Martin, *Nucl. Instrum. Methods* **124**, 329 (1975).
- ¹⁸F. W. Martin and R. K. Cacak, *J. Phys. E* (to be published).
- ¹⁹A. P. Lukirskii, E. P. Savinov, O. A. Ershov, and Yu. F. Shepelev, *Opt. Spektrosk.* **16**, 310 (1964) [*Opt. Spectrosc.* **16**, 168 (1964)]; W. C. Walker, O. P. Rustgi, and G. L. Weissler, *J. Opt. Soc. Am.* **49**, 471 (1959).
- ²⁰Reference 18, Eq. (30), with ω changed to τ for clarity.
- ²¹J. B. Marion and F. C. Young, *Nuclear Reaction Analysis, Graphs, and Tables* (Wiley, New York, 1968), p. 154.
- ²²See, for example, R. B. Leighton, *Principles of Modern Physics* (McGraw-Hill, New York, 1959), p. 493.
- ²³A. Langenberg and J. Van Eck, *Phys. Rev. Lett.* **31**, 71 (1973).
- ²⁴L. H. Toburen, *Phys. Rev. A* **5**, 2482 (1972).
- ²⁵Reference 18, Eq. (4).
- ²⁶L. C. Northcliffe and R. F. Schilling, *Nucl. Data A* **7**, 233 (1970).
- ²⁷Reference 18, Eq. (31).
- ²⁸B. L. Henke, *Adv. X-Ray Anal.* **7**, 460 (1965); see p. 468.
- ²⁹F. Bassani and G. P. Parravicini, *Nuovo Cimento B* **50**, 95 (1967).
- ³⁰J. E. Holliday, *J. Appl. Phys.* **38**, 4720 (1967); J. E. Holliday, in *Soft X-Ray Band Spectra*, edited by D. J. Fabian (Academic, New York, 1968), p. 101; energies and intensities taken from Fig. 16.
- ³¹T. Sagawa, *J. Phys. Soc. Jpn.* **21**, 49 (1966); energies and intensities chosen visually from Fig. 3 and the Fermi edge quoted at 285.6 eV.
- ³²C. A. Coulson and R. Taylor, *Proc. Phys. Soc. Lond. A* **65**, 815 (1952).
- ³³N. Stolterfoht, D. Schneider, and K. G. Harrison, *Phys. Rev. A* **8**, 2363 (1973).
- ³⁴N. Stolterfoht, *Phys. Lett. A* **41**, 400 (1972).
- ³⁵J. McWhorter, D. K. Olsen, H. H. Wolter, and C. F. Moore, *Phys. Rev. A* **10**, 200 (1974).
- ³⁶M. R. C. McDowell and J. P. Coleman, *Introduction to the Theory of Ion-Atom Collisions* (American Elsevier, New York, 1970), p. 181.
- ³⁷D. R. Bates and R. McCarroll, *Proc. R. Soc. A* **245**, 175 (1958); for a treatment in center-of-mass coordinates, see Ref. 36, p. 156.
- ³⁸Reference 2, p. 165.
- ³⁹Reference 21, p. 42.
- ⁴⁰F. W. Martin and J. R. Macdonald, *Phys. Rev. A* **4**, 1974 (1971).
- ⁴¹J. C. Slater, *Phys. Rev.* **36**, 57 (1930), wherein $Z_K = Z - 0.3$ and $Z_L = Z - 4.15$.
- ⁴²W. E. Meyerhof, *Phys. Rev. A* **10**, 1005 (1974).
- ⁴³K. Taulbjerg, B. Fastrup, and E. Laegsgaard, *Phys. Rev. A* **8**, 1814 (1973); K. Taulbjerg and P. Sigmund, *Phys. Rev. A* **5**, 1285 (1972) (see Fig. 1).
- ⁴⁴J. M. Kahn, D. L. Potter, R. D. Worley, *Phys. Rev.* **139**, A1735 (1965).
- ⁴⁵K. G. Harrison, H. Tawara, and F. J. De Heer, *Physica (Utr.)* **66**, 16 (1973) (see Fig. 5).
- ⁴⁶J. H. Macek and J. S. Briggs, *J. Phys. B* **6**, 841 (1973).
- ⁴⁷R. Laubert, H. Haselton, J. R. Mowat, R. S. Peterson, and I. A. Sellin, *Phys. Rev. A* **11**, 135 (1975).
- ⁴⁸These findings were previously described by R. K. Cacak, S. S. Choe, and F. W. Martin, *Bull. Am. Phys. Soc.* **18**, 1508 (1973); F. W. Martin and R. K. Cacak, *ibid.* **20**, 638 (1975); R. K. Cacak and F. W. Martin, *ibid.* **20**, 639 (1975); and F. W. Martin and R. K. Cacak, *ibid.* **20**, 676 (1975).